Role of histidine for charge regulation of unstructured peptides at interfaces and in bulk.

Kurut Sabanoglu, Anil; Henriques, Joao; Forsman, Jan; Skepö, Marie; Lund, Mikael

Published in:
Proteins

DOI:
10.1002/prot.24445

2014

Role of Histidine for Charge Regulation of Unstructured Peptides at Interfaces and in Bulk

Anıl Kurut,* João Henriques, Jan Forsman, Marie Skepö, and Mikael Lund

Division of Theoretical Chemistry, Lund University, P.O.B. 124, SE-22100 Lund, Sweden

E-mail: anil.kurut@teokem.lu.se

Running Title: Histidines Promote Adsorption of Unstructured Peptides

Key words: histidine richness; antimicrobial activity; adsorption of unstructured proteins; Monte Carlo simulations; charge regulation; specific metal binding.

Abstract

Histidine rich, unstructured peptides adsorb to charged interfaces such as mineral surfaces and microbial cell membranes. At a molecular level, we investigate the adsorption mechanism as a function of pH, salt, and multivalent ions showing that (1) proton charge fluctuations are – in contrast to the majority of proteins – optimal at neutral pH, promoting electrostatic interactions with anionic surfaces through charge regulation, and (2) specific zinc(II)-histidine binding competes with protons and ensures an unusually constant charge distribution over a broad pH interval. In turn this further enhances surface adsorption. Our analysis is based on atomistic molecular dynamics simulations, coarse grained Metropolis Monte Carlo, and classical polymer density functional theory. This multi-scale modelling provides a consistent picture in good agreement with experimental data on *Histatin 5*, an antimicrobial salivary peptide. Biological function is discussed and we suggest that charge regulation is a significant driving force for the remarkably robust activity of histidine rich antimicrobial peptides.

*To whom correspondence should be addressed

Introduction

Nature has produced a number of bio-molecules rich in histidines (HIS). These include globular proteins such as hisactophilin and histidine-rich glycoprotein, but also intrinsically disordered peptides (IDPs) such as the histatins. The latter are characterized by lack of stable tertiary structure when the protein exists as an isolated polypeptide under in vitro physiological conditions. It has recently been shown that approximately 30% of all proteins in eukaryotic organisms belong to this group and that IDPs are involved in a large number of central biological processes and diseases.[1] This discovery challenges the traditional protein structure paradigm, which states that a specific well-defined structure is required for correct function. Biochemical evidence has since shown that IDPs are functional, and that lack of folded structure is in fact related to function.[2,3]

Histatins are saliva peptides with multifunctionality. They protect the oral environment against microbial attack, but are also involved in the formation of protective films on solids which is important for the maintenance of oral health and surface integrity. The formation of the acquired tooth enamel pellicle involves the selective adsorption of salivary macromolecules onto the enamel surface. This conditioning film acts as a selective permeability barrier between the tooth surface and the oral environment and regulates the defence against enamel demineralization. It is hence crucial to understand how lack of structure relates to function when adsorbed to exposed biological interfaces. While we in this paper focus on the antimicrobial activity of Histatin5 (His5), we emphasize that our arguments can be generally applied to biomolecular surface adsorption.

His5 consists of 24 amino acids and is the most active member of the histatins against pathogenic yeast *Candida Albicans*.[4] Its antimicrobial activity and possible killing mechanisms are therefore subject to much scientific attention.[5–9] Contrary to many antimicrobial peptides, His5 penetrates the cell membrane without causing membrane rupture which is attributed to its histidine richness.[10,11] Further, histidines (HIS) form complexes with zinc ions[12,13] which promote adsorption to bilayer vesicles[6] as well as its killing activity.[9] It has also been shown that the 16 C-terminal amino acids with a 60% of HIS content, are the active segment of His5,[14] supporting the importance of HIS in the activity.

Accepting that both microbial cell membranes and tooth enamel represent negatively charged interfaces we here investigate the role of histidine on the anionic surface adsorption of a flexible peptide, exemplified by His5. Our theoretical analysis is based on three levels of detail entailing (i) atomistic bulk simulations, (ii) a flexible amino acid bead model with Debye-Hückel electrostatics, and (iii) classical polymer density functional theory. Common for all models is that pH is kept *constant* meaning that the peptide protonation state can fluctuate and respond to the local chemical environment. This gives rise to charge regulations mechanisms[15–17] that may contribute to intermolecular interactions in biomolecular systems – for a recent review, see reference.[18] As will be shown, charge regulation becomes important for histidine-rich biomolecules close to neutral pH. We further investigate how binding metal ions such as zinc influence the adsorption free energy to charged surfaces using an empirical ion-binding potential.

The paper is organized as follows: First we present the three theoretical models and proceed to study bulk electrostatic and structural properties of His5. We then study the adsorption mechanism and free energy as a function of pH and salt concentration. Finally, we discuss the effect of multivalent ions, including specific metal binding and possible implications for biological activity.

Protein Models and Methods

We have used three models with different levels of detail (Figure 1), one atomistic and two coarse grained (CG), with a common feature of fluctuating charges on basic and acidic residues. That is, the *chemical potential* of protons is kept constant during the simulation, contrasting most simulation work where partial charges are fixed. Atomistic level Molecular Dynamics (MD) simulations is used to investigate bulk properties of His5 and to verify that the CG models capture the essential physical features. Monte Carlo simulations and an amino acid bead model are used to investigate both bulk properties and surface affinities. Since atomistic MD requires substantial computational resources we have used this method only to scan a limited parameter range while fine scanning has been done using a much faster CG model. Finally we have tested hard-sphere amino acid bead

model using classical polymer density functional theory (DFT) which are well suited for further adsorption studies in concentrated solutions.

Coarse grained Monte Carlo simulations

Model

Histatin 5 is modeled as a flexible chain where each residue is coarse grained into a sphere and connected with harmonic bonds[19] – see Figure 1. The amino acid radii are determined from their molecular weight by assuming a common density of 0.9 g/ml. During the simulations, the charges of basic and acidic amino acids as well as C and N terminals are allowed to fluctuate according to pH, when $\xi_{reg} = 1$ in Eq. 1. An average bulk charge is assigned to each site when $\xi_{reg} = 0$. Water and monovalent ions are treated implicitly while divalent ions are explicitly represented by spheres with a 2 Å radius.[20]

In addition to proton binding we also mimic specific zinc coordination to deprotonated HIS using a short range (SR) square-well attraction, adjusted to 1.2×10^5 M^{-1}, the experimental binding constant of zinc to isolated imidazole groups[13] – see Table I and Eq. 1. The attraction range of 2.4 Å is the average distance between Zn^{2+} and HIS in three different zinc binding proteins (PDBs 2XQV, 2XY4, 2WB0, 2IIM).

The system energy for a given configuration is

$$
\begin{aligned}
U_{tot} = & \overbrace{\left(4\varepsilon \sum_{i>j}^{n} \left(\frac{\sigma_{ij}}{r_{ij}}\right)^{12} - \left(\frac{\sigma_{ij}}{r_{ij}}\right)^{6}\right)}^{\text{Lennard-Jones (LJ)}} \\
& + \underbrace{\left(\frac{1}{4\pi\varepsilon_0\varepsilon_r} \sum_{i>j}^{n_t} \frac{q_i q_j}{r_{ij}} e^{-\kappa r_{ij}}\right)}_{\text{Debye-Hückel}} \\
& + \underbrace{\left(\xi_{reg} k_B T \sum_{1}^{n_p} (\mathrm{p}K_a - \mathrm{pH}) \ln(10)\right)}_{\text{Intrinsic titration energy}} \\
& + \underbrace{\left(\xi_{surf} \sum_{i}^{n_t} q_i \Phi_0 e^{-\kappa d_i}\right)}_{\text{Gouy-Chapman (G-C)}} + \underbrace{\left(\sum_{i}^{n_b} \frac{1}{2} k_h (R_i - Re)^2\right)}_{\text{Harmonic Bond}} \\
& + \underbrace{\left(\sum_{1}^{n_H} -\varepsilon_{Zn} (d_{Zn-H} < 2.4)\right)}_{\text{short range attraction (SR)}}
\end{aligned}
\tag{1}
$$

where all the parameters are given in Table I.

Method

A single peptide is simulated using the Metropolis Monte Carlo (MC) algorithm in the canonical ensemble (NVT) at 298 K in a volume of 300x300x300 Å^3 and 300x300x150 Å^3 for bulk and surface adsorption studies, respectively. In bulk studies ($\xi_{surf} = 0$), periodic boundaries are applied in all directions whereas in adsorption simulations ($\xi_{surf} = 1$), a uniform surface charge density is assigned to the $+xy$ wall and hard boundaries are applied in the z direction. Chain conformations are sampled using crankshaft, pivot, branch rotations, reptation and single monomer MC moves together with whole chain rotation and translation. All MC simulations are performed using the Faunus framework.[21]

Atomistic constant-pH MD simulations

Model

A modified version of the GROMOS 54A7 force field[22] is used for the atomistic description of His5. All simulations are started with a linear structure of His5, built using MacPyMOL.[23] The charges of 20 sites, including N and C terminals, are updated during the simulations – see next section.

Method

All constant-pH MD simulations are performed using the stochastic titration method[24–31] which relies on three steps. First, the protonation states of residues are determined using Poisson-Boltzmann/Monte Carlo (PB/MC) calculations. Second, the solvent is relaxed around the frozen peptide using a short MD simulation. The third step is an MD simulation of the unrestraint system. All simulations are performed in the isobaric-isothermal ensemble (NPT), at 300 K and 1 bar with the GROMACS 4.0.7 distribution.[32–35] PB and MC calculations are performed with MEAD[36] and PETIT[37,38] softwares, respectively. The simulations are run for 20 ns in triplicate and the last 15 ns of each replica is used for the analysis. To confirm the convergence of the structural properties, two independent replica-exchange MD (REMD) simulations in temperature are performed with 64 replicas, each in a salt free solution at pH 7 – see supporting information.

Density functional theory

Classical polymer density theory (DFT) was originally developed by Woodward,[39] and has seen subsequent developments and extensions. We shall refrain from a complete description here, and instead refer to a recent work,[20] where a rather general exposition is provided. In this work, we have used a version of the implicit solvent approach, denoted "model II" in ref.[40] However, we will here also (approximately) account for differences in size between monomers (coarse-grained amino acids) and solvent particles (water). Given the minor role of dispersion (Lennard-Jones)

interactions in our system, these are neglected in the DFT approach. Tests have confirmed that the Lennard-Jones interactions have a negligible influence on the results. Moreover, the CG amino acid monomers have a common (hard-sphere) diameter of $d_m = 6.2$ Å, which is the average value in the soft sphere CG model. The neighboring monomers are connected by stiff bonds with a fixed length of 5 Å. The solvent particles enter explicitly via a net incompressibility constraint (see ref[40]): $n_t = n_m \gamma d_m^3 + n_s d_s^3$ where n_m and n_s are solvent and monomer densities, and we have simply set $n_t = 1$ corresponding to simple cubic close packing. The parameter γ accounts for the reduction in excluded volume brought about by bonding (connected spheres exclude less volume than free ones). According to Hall et al,[41] this factor can be estimated to about 0.63, for a pearl-necklace chain. Woodward, on the other hand, found an empirical value of 0.83. In our case, with fused hard-sphere chains, this would be reduced somewhat. Given that we work with a rather crude model anyway, with excluded volume interactions playing a minor role, we chose to simply set $\gamma = 0.65$, which might be a reasonable compromise of all these considerations. We have made tests to ensure that our findings and conclusions are insensitive to the specific value of γ.

Note that the polymer DFT is *exact* for the case of non-interacting monomers. In order to treat titrations properly, the two different states of the monomers (charged/uncharged) must be properly accounted for, according to the prescription described in ref.[40]

Analysis

We have analyzed statistical mechanical averages of the residual charges $\langle z_i \rangle$, the net charge of His5, $Z = \Sigma_i \langle z_i \rangle$, the end-to-end distance $R_{e2e}^2 = \langle r_{1,last}^2 \rangle$, radius of gyration, $R_g^2 = \frac{\Sigma_i m_i \langle r_{i,cm}^2 \rangle}{\Sigma_i m_i}$ where $r_{i,cm}$ is the distance between residue i and the mass center of His5 as a function of the center of mass distance from the surface. The charge capacitance is analyzed using the fluctuations of the net charge, $C = \langle Z^2 \rangle - \langle Z \rangle^2 = -\frac{\partial Z k_B T}{\partial e \Phi}$ where Φ is the external electric potential from the surface. Probability density functions with respect to distance from the surface are sampled using the histogram method and normalized such that the integral yields the average monomer concentration times the z-box length ($26 \times 150/(300 \times 300 \times 150)$, number/Å^2).

The analyses of the MD simulations have been done using GROMACS 4.0.7 software package[32–35] and in-house tools. The calculations of correlation-corrected errors for averages over a single simulation replicate have been computed using standard methods.[42] The final errors of the averages over replicates have been computed using the law of total variance.

Results and Discussion

Bulk properties

The bulk properties of His5 in dilute solutions have been investigated as a function of monovalent salt concentration and pH. To mimic biological conditions, ionic strengths of 80 and 150 mM were chosen while, for completeness, we also include the salt free case.

Electrostatic Properties

As shown in Figure 2 (left), the isoelectric point (pI) of His5 is predicted to 10.5 by both MC and MD simulations, coinciding with previous theoretical studies.[11,43] Calculated net charges using both models are in a good agreement over the whole pH range. At extreme acidic and basic conditions, the net charge reaches +15e and -5e, respectively and contrary to most proteins and peptides, His5 is cationic over a wide pH range. At intermediate and high ionic strengths, the reduced electrostatic repulsion due to salt screening enables protonation of nearby basic residues and allows for a higher net charge.

Charge fluctuations result in a high charge capacitance (see Eq. 1) and hence, a high charge regulation ability. That is, the molecular charge may readily respond to an external electric field by taking up or releasing protons. As shown in Figure 2, the capacitance of His5 has four maxima and three minima. In this study, we focus on the biological pH range. At salt free conditions, the peak and the minimum are located at pH 5 and 7, respectively, meaning that the charge distribution can be easily perturbed at pH 5 but not at pH 7. Although the capacitance extrema predicted by MD are at slightly lower pH, both models agree on the shift of these extrema to higher pH with

increasing ionic strength and on the capacitance minimum around pH 8.

To determine which residues contribute to the capacitance peak, we investigate the residual stoichiometric acid dissociation constant (pK_a^*) obtained from the titration curve of each residue. At pH=pK_a^*, a residue has high charge fluctuations due to equally probable protonation states, leading to a capacitance peak. Table II shows that the peak around pH 6 originates from HIS residues with pK_a^* ranging from 5.4 to 6.2. At pH 8, only the N-terminal contributes slightly to the capacitance, thus leading to a minimum.

Structural Properties

Although atomistic and coarse grained models agree well on the electrostatic properties, they differ slightly on the structure predictions. As seen in Figure 2, the atomistic model favors more compact conformations than the CG model, resulting in a smaller gyration radius, R_g. This can be due to smaller excluded atom volumes combined with hydrogen bonds. In the CG flexible chain models, the high entropic cost of compact conformations combined with lack of hydrogen bonds favors random coil conformations, and thus larger R_g. Experimental studies[11,14,44] have shown that besides $\beta-$turns, His5 lacks secondary structure in aqueous solution, thus supporting the CG models. Nevertheless, the true R_g is probably in between and both models still predict the same relative changes in R_g induced by salt and pH – see Figure 2.

Interaction with negative surfaces

Effect of charge regulation

While most proteins have capacitance peaks around pH 4,[45] we here show that the capacitance peak of His5 is at pH 6 coinciding with normal saliva. This implies that HIS provides a significant ability to adjust the net charge in the vicinity of a negative microbial membrane. Figure 3 shows that His5 becomes more positively charged while approaching a negative surface at pH 6. Since this cationic gain depends on the number of residues with $pK_a^* = $ pH, the abundance of HIS provides

an additional charging capacity up to $3e$ and enhances the affinity to the surface (see Figure 3, bottom). In contrast, the lack of residues with $pK_a^* \approx 8$ results in a slight net charge increase and the surface affinity is thus unaffected.

Note that the charge regulation may also lead to *neutralization* of the peptide. His5 penetrates cells without deforming the membrane integrity[7,10,46] and bearing charges while passing the apolar membrane interior may be costly. With its high capacitance, HIS, may lower this free energy cost by adapting the deprotonated state, thus avoiding pore formation on the membrane.

Effect of pH

The high positive charge at pH 6 combined with charge regulation results in a strong adsorption to the negative surface – see Figure 3. Due to the release of protons, this adsorption is reduced at alkaline conditions but at low ionic strengths, the surface adsorption is still significant. In contrast, the interaction free energy at low pH reaches 8.5 k_BT with a free energy minimum closer to the surface hinting at irreversible adsorption with a more compact adsorbed layer.

Effect of monovalent salt

As seen in Figure 3, the surface affinity of His5 decreases with increasing monovalent salt concentration due to the screening of electrostatic attraction. Although salt is also reducing the repulsion within the peptide, thus allowing higher net charges, this effect is insufficient to compensate for the screened surface attraction. Our model predicts a clear correlation between ionic strength and surface affinity and is thus consistent with experiments showing that the biological activity of His5 diminishes with increasing ionic strength.[11,47]

Adsorption Mechanism

To determine the adsorption mechanism we have investigated the gyration radius, R_g, and the distribution of individual residues while His5 approaches the surface. As seen in Figure 4, the electric field from the surface induces conformational changes on His5 when the separation is

smaller than 40 Å. The z-component of R_g first increases indicating a chain elongation towards the surface, followed by a contraction due to xy-stretching of the adsorbed chain on the surface. The elongation is reflected as a depletion of some residues from the bulk – see Figure 4. These residues, containing two positive ARG-LYS patches, drive the peptide to the surface and mediate the adsorption by providing two grafting regions. The primary ARG-LYS patch consists of the 11^{th} to 13^{th} residues and provides the strongest attachment.

Conformational entropy drives the N (NTR) and C (CTR) terminal domains further from the surface. However, the energetic gain of positioning the NTR and the nearby secondary ARG-LYS patch close to the surface, partly compensates for this entropy and the NTR consequently adsorbs stronger than the CTR.

Many antimicrobial salivary peptides, including histatins, are expressed by multiple gene families.[48] Diversities in these families cause polymorphism which may influence the microbial activity.[49] For instance, a rare variant of proline-rich glycoprotein does not bind to bacteria.[50] We have tested the sensitivity of the primary grafting patch to a point mutation by replacing the 12^{th} ARG with a negative TYR. This mutation eliminates the grafting to the surface (Figure 6) resulting in a 40 % reduction in the overall surface affinity – see Figure 5. In addition, mutating the positive primary ARG-LYS patch to a neutral GLY completely prevents adsorption of this region and supports the possible suppression of interactions with microbial membranes due to protein polymorphism.

Due to HIS attraction, the adsorption of CTR persists even when the primary patch is completely desorbed (Figure 6), indicating the prominent role played by histidines. An experimental study of His5 fragments[14] showed that the HIS residues in the CTR domain and the primary ARG-LYS patch are the active parts. This supports our predictions and the importance of electrostatics for antimicrobial activity.

Effect of pH

As seen in the residue concentration profiles (Figure 7), increasing pH from 6 to 7, dramatically reduces the surface affinity of HIS and results in a weaker adsorption of both ARG-LYS patches

and the CTR. This is more pronounced at pH 8 where the CTR completely desorbs from the surface due to lack of charge regulation combined with released protons. Although the ARG-LYS patches are still positive at this pH, their affinity to the surface is insufficient to compensate conformational entropy loss of the terminals, thus leading to desorption of both terminals and the secondary ARG-LYS patch. This gradual desorption can be seen in Figure 8 where we have plotted the most probable residue positions relative to the surface.

Previous reports show that the activity of His5 is independent of pH.[47,51] However, in these studies, the pH dependence was investigated at low ionic strength ($\sim$10 mM) where arginine and lysine dominate the surface attraction. We here show that even at 80 mM ionic strength – see Figure 3, His5 has appreciable affinity to the surface, independent of the studied acidic conditions. This suggests that His5 is active against microbes once its surface affinity is above a critical value. Further, our results indicate that the surface affinity of His5 is sensitive to pH changes in environments where the ionic strength is relatively high (such as saliva). As will be shown, this statement is valid only for zinc-free conditions.

Note that the surface is modeled independently of solution conditions with a constant surface charge density. In reality, the phosphate groups of microbial membranes may change their protonation state according to pH. Our model may therefore slightly underestimate the surface affinity with increasing pH.

Effect of monovalent salt

The residue concentration profiles in Figure 7 show that adsorption of all residues is reduced with increasing salt concentration. The most pronounced salt screening effect is observed on the adsorption of the CTR domain at pH 7 and 8 where charge regulation effects are of little importance – see Figure 8. In contrast, at pH 6, the cooperation between positive patches and the charge regulation of HIS partly compensates salt screening and provides sufficient attraction to preserve the peptide conformation at the surface. These adsorption features are also captured by DFT as shown in the supporting information.

Effect of charge regulation

To estimate the importance of charge regulation, we have investigated the residue profiles with and without charge regulation. The latter is performed by assigning bulk charge to each residue corresponding to a certain pH. As seen in Figure 9, all profiles *except* for HIS are mostly unaffected by charge regulation. The surface affinity of HIS without additional regulated charges is insufficient to compensate for the conformational entropy loss, resulting in weaker adsorption of CTR as well as the secondary ARG-LYS patch – see also Figure 7. This emphasizes the importance of charge regulation on the CTR adsorption, the active part of His5, and potentially on biological activity. In the present example the charge regulation mechanism is important within a nanometer from the surface while direct electrostatic attraction with arginine and lysine are of longer range (first order vs. second order multipole electrostatics[15]). Thus LYS and ARG cause a long range attraction while charge regulation of HIS enhances the adsorption at short separations and at low pH. This is consistent with recent experimental work mapping the roles played by LYS and ARG.[52]

Effect of divalent ions

Non-binding ions

In addition to monovalent ions, biological environments contain divalent metal ions such as magnesium, zinc, and calcium.[48] Taking saliva as an example, Ca^{2+} is the most abundant divalent ion[48] and its concentration depends on the oral health state.[53,54] Since high levels of divalent ions may lead to ion correlations,[55] we investigated how Ca^{2+} affects the surface affinity of His5. Note that calcium does not bind *specifically* to His5 and will here be representative of any generic divalent ion. Simulations are performed at 6.15 mM of Ca^{2+} corresponding to an elevated saliva level[48] with *explicit* divalent and *implicit* monovalent ions. This hybrid model has previously been shown to correctly reproduce electrostatics in strongly coupled systems.[20] For comparison with the monovalent salt studies in previous sections, the total ionic strength is kept constant at 80 mM. As seen in Figure 10, the adsorption and charge regulation of His5 are unaffected by Ca^{2+} ions

at 80 mM ionic strength indicating that calcium induces no or only weak correlation effects and behaves chiefly as an ionic screening agent like monovalent ions.

Binding ions

Contrary to calcium, zinc(II) selectively coordinates to the imidazole group of HIS[12,13] with one Zn^{2+} ion chelating up to four HIS.[56] It has been shown that this binding promotes the activity of His5 by facilitating the adsorption to microbial membranes and inducing fusion.[6,9] To mimic zinc binding, we have investigated the surface affinity of His5 in the presence of explicit zinc ions with a specific short range attraction to HIS as detailed in the model section. Simulations are performed with two Zn^{2+} ions corresponding to 0.25 mM to allow all possible zinc coordinations. Although this concentration is higher than salivary levels (μM),[57] it is still relevant to biological applications including usage of dental products with zinc salts which may bring the oral zinc level up to 0.5 mM.[58] As seen in Figure 10, the surface affinity of His5 is enhanced by zinc at pH > 6 where protons are unable to compete for zinc binding sites. In contrast, at pH 6 or lower, this competition is won by protons, rendering the charge distribution oblivious to the presence of zinc. Our results are in line with experimental studies showing that His5 forms strong metal-peptide complexes at neutral and basic conditions.[59] Finally, Figure 10 shows a reduction in gyration radius upon adsorption, suggests that zinc complexation induces compact conformations, which are also observed experimentally,[59] via bridging HIS – see snapshots in Figure 11. Interestingly, zinc complexation leads to a strong adsorption *independent* of pH by providing more grafting points on the surface and restoring positive charges lost from proton release.

Conclusion

Focusing on electrostatics, we have investigated bulk properties of an unstructured histidine rich peptide, histatin 5, as well as its adsorption to a uniformly charged surface to determine the role of histidines. In bulk solution, coarse grained and atomistic models have been explored using Monte

Carlo and Molecular Dynamics simulations. All models quantitatively agree on bulk electrostatics indicating that a sufficient level of detail is included in the CG models. Qualitative agreement is obtained on structural properties by predicting the same pH and salt dependence, suggesting that the effect of pH and salt can be captured without full atomic detail.

We show that histatin 5 has an uncommonly high charge capacitance at pH 6 due to a high histidine content. Matching capacitance peak conditions activates a charge regulation mechanism and turns histidines into positive charge providers under an external electric field. This mechanism can be generalized to any titratable sites of any proteins, regardless of size and structure, with matching pK_a and pH. While charge regulation promotes adsorption at pH 6, increasing pH causes proton release and consequently desorption of His5. However, at pH > 6, deprotonated histidines act as zinc chelators that restore the positive charges lost from proton release. In effect, the pH sensitivity is eliminated and zinc thus ensures a robust, pH independent surface affinity. Finally, charge regulation may neutralize the peptide, thereby preventing unfavorable desolvation interactions while passing bilayers. This mechanism may highlight why His5 can penetrate microbial cells without rupturing their membranes.

Acknowledgement

For financial support and computational resources we thank the eSSENCE strategic program, Sweden's Innovation Agency "Vinnova", the Linneaus Center of Excellence "Organizing Molecular Matter" and LUNARC, Lund, Sweden. We also thank Chris H.J. Evers for piloting this study.

References

(1) Wright, P. E.; Dyson, H. Intrinsically unstructured proteins: re-assessing the protein structure-function paradigm. *Journal of Molecular Biology* **1999**, *293*, 321–331.

(2) Ward, J.; Sodhi, J.; McGuffin, L.; Buxton, B.; Jones, D. Prediction and Functional Analysis of

Native Disorder in Proteins from the Three Kingdoms of Life. *Journal of Molecular Biology* **2004**, *337*, 635–645.

(3) Liu, J.; Faeder, J. R.; Camacho, C. J. Toward a quantitative theory of intrinsically disordered proteins and their function. *Proceedings of the National Academy of Sciences* **2009**,

(4) Kavanagh, K.; Dowd, S. Histatins: Antimicrobial Peptides with Therapeutic Potential. *J. Pharm. Pharmacol.* **2004**, *56*, 285–289.

(5) Tsai, H.; Bobek, L. Human Salivary Histatins: Promising Anti-Fungal Therapeutic Agents. *Crit. Rev. Oral Biol. Med.* **1998**, *9*, 480–497.

(6) Melino, S.; Rufini, S.; Sette, M.; Morero, R.; Grottesi, A.; Paci, M.; Petruzzelli, R. Zn(2+) Ions Selectively Induce Antimicrobial Salivary Peptide Histatin-5 To Fuse Negatively Charged Vesicles. Identification And Characterization Of A Zinc-Binding Motif Present In The Functional Domain. *Biochemistry* **1999**, *38*, 9626–9633.

(7) Den Hertog, A.; Van Marle, J.; Van Veen, H.; Van't Hof, W.; Bolscher, J.; Veerman, E.; Amerongen, A. Candidacidal Effects Of Two Antimicrobial Peptides: Histatin 5 Causes Small Membrane Defects, But Ll-37 Causes Massive Disruption Of The Cell Membrane. *Biochem. J.* **2005**, *388*, 689.

(8) Dong, J.; Vylkova, S.; Li, X.; Edgerton, M. Calcium Blocks Fungicidal Activity of Human Salivary Histatin 5 through Disruption of Binding with Candida albicans. *J. Dent. Res.* **2003**, *82*, 748–752.

(9) Rydengård, V.; Andersson Nordahl, E.; Schmidtchen, A. Zinc Potentiates The Antibacterial Effects Of Histidine-Rich Peptides Against Enterococcus Faecalis. *FEBS J.* **2006**, *273*, 2399–2406.

(10) Luque-Ortega, J. R.; van't Hof, W.; Veerman, E. C. I.; Saugar, J. M.; Rivas, L. Human An-

timicrobial Peptide Histatin 5 Is A Cell-Penetrating Peptide Targeting Mitochondrial Atp Synthesis In Leishmania. *FASEB J.* **2008**, *22*, 1817–1828.

(11) Helmerhorst, E. J.; van't Hof, W.; Breeuwer, P.; Veerman, E. C.; Abee, T.; Troxler, R. F.; Amerongen, a. V.; Oppenheim, F. G. Characterization Of Histatin 5 With Respect To Amphipathicity, Hydrophobicity, And Effects On Cell And Mitochondrial Membrane Integrity Excludes A Candidacidal Mechanism Of Pore Formation. *J. Biol. Chem.* **2001**, *276*, 5643–5649.

(12) Grogan, J.; McKnight, C. J.; Troxler, R. F.; Oppenheim, F. G. Zinc And Copper Bind To Unique Sites Of Histatin 5. *FEBS Lett.* **2001**, *491*, 76–80.

(13) Gusman, H.; Lendenmann, U.; Grogan, J.; Troxler, R. F.; Oppenheim, F. G. Is Salivary Histatin 5 A Metallopeptide? *Biochem. Biophys. Acta* **2001**, *1545*, 86–95.

(14) Raj, P. a.; Edgerton, M.; Levine, M. J. Salivary Histatin 5: Dependence Of Sequence, Chain Length, And Helical Conformation For Candidacidal Activity. *J. Biol. Chem.* **1990**, *265*, 3898–905.

(15) Kirkwood, J. G.; Shumaker, J. B. Forces Between Protein Molecules in Solution Arising from Fluctuations in Proton Charge and Configuration. *Chemistry* **1952**, *38*, 863–871.

(16) Wyman, J.; Gill, S. J. *Binding and Linkage: Functional Chemistry of Biological Macromolecules*; University Science Books: Mill Valley, 1990; p 330.

(17) Kao, Y.-H.; Fitch, C. A.; Bhattacharya, S.; Sarkisian, C. J.; Lecomte, J. T.; Garcia-Moreno E., B. Salt Effects on Ionization Equilibria of Histidines in Myoglobin. *Biophysical Journal* **2000**, *79*, 1637–1654.

(18) Lund, M.; Jönsson, B. Charge regulation in biomolecular solution. *Quarterly Reviews of Biophysics* **2013**, *in press, doi:10.1017/S003358351300005X*.

(19) Evers, C. H. J.; Andersson, T.; Lund, M.; Skepö, M. Adsorption of Unstructured Protein β-Casein to Hydrophobic and Charged Surfaces. *Langmuir* **2012**, *28*, 11843–9.

(20) Forsman, J.; Nordholm, S. Polyelectrolyte mediated interactions in colloidal dispersions: hierarchical screening, simulations, and a new classical density functional theory. *Langmuir* **2012**, *28*, 4069–79.

(21) Lund, M.; Trulsson, M.; Persson, B. Faunus: An object oriented framework for molecular simulation. *Source Code for Biology and Medicine* **2008**, *3:1*.

(22) Schmid, N.; Eichenberger, A.; Choutko, A.; Riniker, S.; Winger, M.; Mark, A.; Van Gunsteren, W. Definition and testing of the GROMOS force-field versions 54A7 and 54B7. *Eur. Biophys. J.* **2011**, 1–14.

(23) Schrödinger, 2012; MacPyMOL: PyMOL Enhanced for Mac OS X.

(24) Baptista, A.; Teixeira, V.; Soares, C. Constant-pH molecular dynamics using stochastic titration. *J. Chem. Phys.* **2002**, *117*, 4184–4200.

(25) Machuqueiro, M.; Baptista, A. Constant-pH molecular dynamics with ionic strength effects: protonation-conformation coupling in decalysine. *J. Phys. Chem. B* **2006**, *110*, 2927–2933.

(26) Machuqueiro, M.; Baptista, A. The pH-dependent conformational states of kyotorphin: a constant-pH molecular dynamics study. *Biophys. J.* **2007**, *92*, 1836–1845.

(27) Machuqueiro, M.; Baptista, A. Acidic range titration of HEWL using a constant-pH molecular dynamics method. *Proteins: Struct., Funct., Bioinf.* **2008**, *72*, 289–298.

(28) Machuqueiro, M.; Baptista, A. Molecular dynamics at constant pH and reduction potential: application to cytochrome c 3. *J. Am. Chem. Soc.* **2009**, *131*, 12586–12594.

(29) Campos, S.; Machuqueiro, M.; Baptista, A. Constant-pH molecular dynamics simulations reveal a β-rich form of the human prion protein. *The J. Phys. Chem. B* **2010**,

(30) Machuqueiro, M.; Baptista, A. Is the prediction of pKa values by constant-pH molecular dynamics being hindered by inherited problems? *Proteins: Struct., Funct., Bioinf.* **2011**,

(31) Vila-Viçosa, D.; Campos, S.; Baptista, A.; Machuqueiro, M. Reversibility of Prion Misfolding: Insights from Constant-pH Molecular Dynamics Simulations. *J. Phys. Chem. B* **2012**,

(32) Berendsen, H.; van der Spoel, D.; van Drunen, R. GROMACS: A message-passing parallel molecular dynamics implementation. *Comput. Phys. Commun.* **1995**, *91*, 43–56.

(33) Lindahl, E.; Hess, B.; Van Der Spoel, D. GROMACS 3.0: a package for molecular simulation and trajectory analysis. *J. Mol. Model.* **2001**, *7*, 306–317.

(34) Van Der Spoel, D.; Lindahl, E.; Hess, B.; Groenhof, G.; Mark, A.; Berendsen, H. GROMACS: fast, flexible, and free. *J. Comput. Chem.* **2005**, *26*, 1701–1718.

(35) Hess, B.; Kutzner, C.; Van Der Spoel, D.; Lindahl, E. GROMACS 4: Algorithms for highly efficient, load-balanced, and scalable molecular simulation. *J. Chem. Theory Comput.* **2008**, *4*, 435–447.

(36) Bashford, D.; Gerwert, K. Electrostatic calculations of the pKa values of ionizable groups in bacteriorhodopsin. *J. Mol. Biol.* **1992**, *224*, 473–486.

(37) Teixeira, V.; Cunha, C.; Machuqueiro, M.; Oliveira, A.; Victor, B.; Soares, C.; Baptista, A. On the use of different dielectric constants for computing individual and pairwise terms in Poisson-Boltzmann studies of protein ionization equilibrium. *J. Phys. Chem. B* **2005**, *109*, 14691–14706.

(38) Baptista, A.; Martel, P.; Soares, C. Simulation of electron-proton coupling with a Monte Carlo method: application to cytochrome c3 using continuum electrostatics. *Biophys. J.* **1999**, *76*, 2978–2998.

(39) Woodward, C. E. Density functional theory for inhomogeneous polymer solutions. *J. Chem. Phys.* **1991**, *94*, 3183.

(40) Xie, F.; Woodward, C.; J., F. Fluid-Fluid Transitions at Supercritical Conditions. *Langmuir* **2013**, *29*, 2659.

(41) Dickman, R.; Hall, C. K. Equation of state for chain molecules: Continuous-space analog of Flory theory. *J. Chem. Phys.* **1986**, *85*, 4108.

(42) Allen, M.; Tildesley, D. *Computer simulation of liquids*; Oxford university press, 1989; Vol. 18.

(43) Nikawa, H.; Fukushima, H.; Makihira, S.; Hamada, T.; Samaranayake, L. P. Fungicidal Effect Of Three New Synthetic Cationic Peptides Against Candida Albicans. *Oral Diseases* **2004**, *10*, 221–228.

(44) Raj, P. A.; Marcus, E.; Sukumaran, D. K. Structure Of Human Salivary Histatin 5 In Aqueous And Nonaqueous Solutions. *Biopolymers* **1998**, *45*, 51–67.

(45) Lund, M.; Jönsson, B. On The Charge Regulation Of Proteins. *Biochemistry* **2005**, *44*, 5722–7.

(46) Den Hertog, A. L.; Wong Fong Sang, H. W.; Kraayenhof, R.; Bolscher, J. G. M.; Van't Hof, W.; Veerman, E. C. I.; Nieuw Amerongen, A. V. Interactions Of Histatin 5 And Histatin 5-Derived Peptides With Liposome Membranes: Surface Effects, Translocation And Permeabilization. *Biochem. J.* **2004**, *379*, 665–72.

(47) Xu, T.; Levitz, S. M.; Diamond, R. D.; Oppenheim, F. G. Anticandidal activity of major human salivary histatins. *Infect. Immun.* **1991**, *59*, 2549–2554.

(48) Edgar, M., Dawes, C., O'Mullane, D., Eds. *Saliva and Oral Health*, 3rd ed.; British Dental Association: London, 2004.

(49) Rudney, J. Does Variability in Salivary Protein Concentrations Influence Oral Microbial Ecology and Oral Health? *Crit. Rev. Oral Biol. Med.* **1995**, *6*, 343–367.

(50) Azen, E. A. Genetics of Salivary Protein Polymorphisms. *Crit. Rev. Oral Biol. Med.* **1993**, *4(3/4)*, 479–485.

(51) Kacprzyk, L.; Rydengård, V.; Mörgelin, M.; Davoudi, M.; Pasupuleti, M.; Malmsten, M.; Schmidtchen, A. Antimicrobial Activity Of Histidine-Rich Peptides Is Dependent On Acidic Conditions. *Biochim. Biophys. Acta* **2007**, *1768*, 2667–2080.

(52) Kacprzyk, L.; Rydengård, V.; Mörgelin, M.; Davoudi, M.; Pasupuleti, M.; Malmsten, M.; Schmidtchen, A. Antimicrobial activity of histidine-rich peptides is dependent on acidic conditions. *Biochimica et Biophysica Acta (BBA) - Biomembranes* **2007**, *1768*, 2667 – 2680.

(53) Sah, N.; More, S.; Bhutani, H. Comparision Of Salivary Calcium Levels In Healthy Subjects And Patients With Gingivitis And Periodontitis: A Cross-Sectional Biochemical Study. *ASOR* **2012**, *2(1)*, 13–16.

(54) Hassan, S.; A Al-Sandook, T. Salivary calcium concentration in patients with high incidence of calculus formation. *Al–Rafidain Dent. J.* **2005**, *5*, 88–90.

(55) Guldbrand, L.; Jönsson, B.; Wennerström, H.; Linse, P. Electric double layer forces. A Monte Carlo study. *J. Chem. Phys.* **1984**, *80*, 2221–2228.

(56) Edsall, J. T.; Felsenfeld, G.; Goodman, D. S.; Gurd, F. R. N. The Association of Imidazole with the Ions of Zinc and Cupric Copper. *J. Am. Chem. Soc.* **1954**, *76*, 3054–3061.

(57) Bales, C.; Freeland-Graves, J.; Askey, N.; Behmardi, F.; Pobocik, R.; Fickel, J. J.; Greenlee, P. Zinc, Magnesium, Copper , And Protein Concentrations In Human Saliva : Age- And Sex-Related Differences. *Am. J. Clin. Nutr.* **1990**, *51*, 462–469.

(58) Harrap, G.; Best, J.; Saxton, C. Human Oral Retention of Zinc From Mouthwashes Containing Zinc Salts And Its Relevance to Dental Plaque Control. *Arch. Oral Biol.* **1984**, *29*, 87–91.

(59) Brewer, D.; Lajoie, G. Evaluation Of The Metal Binding Properties Of The Histidine-Rich Antimicrobial Peptides Histatin 3 And 5 By Electrospray Ionization Mass Spectrometry. *Rapid Commun. Mass Spectrom.* **2000**, *14*, 1736–1745.

Figure Legends

Figure 1. Models in decreasing order of detail, left to right: Atomistic (MD), soft sphere amino acid bead model (MC), and hard sphere amino acid model (DFT).

Figure 2. Electrostatic and structural properties of His5 as a function of pH and 1:1 salt concentration calculated using MC (lines) and MD (symbols) simulations. The interval fenced by the dashed lines shows saliva conditions.

Figure 3. Net charge and interaction free energy of His5 as a function of distance from a surface with a charge density $\rho = -300$ Å$^2/e$ with (solid lines) and without (dashed lines) charge regulation at pH 6 and pH 8 where the capacitance is maximized and minimized, respectively.

Figure 4. Residual concentration profile in mM as a function of the distance from the surface at pH 6 and 80 mM 1:1 salt. *Inset*: Radius of gyration and its components with (solid) and without (dashed) charge regulation. Circles indicate the most probable location of each residue relative to the surface and average bulk charges are shown in parentheses.

Figure 5. Interaction free energy of His5 (solid lines), mutant1 (dashed lines, 12-ARG is replaced by a negative TYR) and mutant2 (circles, primary ARG-LYS patch is mutated to a neutral GLY) at pH 6 and 80 mM 1:1 salt solution.

Figure 6. Concentration profiles of mutant1 (*top*) and mutant2 (*bottom*) at pH 6 and 80 mM 1:1 salt solution as a function of the distance from the surface. Mutated amino acids are indicated by *. Circles show the most probable positions of residues relative to the surface.

Figure 7. Residual concentration profile in mM as a function of distance from the surface at pH 6, 7, and 8; in 80 mM and 150 mM 1:1 salt. White and black circles show the most probable

positions of residues relative to the surface predicted by MC and DFT, respectively.

Figure 8. Most probable positions of residues relative to the surface at 80 mM (full symbols) and 150 mM (open symbols).

Figure 9. Difference between the residual concentration profiles with and without charge regulation at pH 6 and 80 mM 1:1 salt solution. The most probable positions of residues with and without charge regulation are shown by black and white circles, respectively.

Figure 10. Properties of His5 as a function of the surface distance at 80 mM total ionic strength with and without divalent ions. See Table III for the concentration of divalent ions.

Figure 11. Concentration profiles of residues with explicit divalent ions at pH 6, 7 and 8 and 80 mM total ionic strength. Deprotonated HIS (red), calcium (yellow) and zinc (blue) ions are shown in the snapshots of His5 conformation on the surface.

Table I: Parameters in Equation 1

Parameter $=$ **Value**	**Description**
$n = 26$	all residues
$\varepsilon = 0.05\ k_BT$	strength of LJ
$\sigma_{ij} = (\sigma_i + \sigma_j)/2$	LJ diameter
$= (4 - 8.2)$ Å	6.2 Å in average
r_{ij}	center of mass distance
e	electron unit charge
ε_0	permittivity of vacuum
$\varepsilon_r = 80$	water dielectric constant
$n_t = 20$	titratable residues
q_i	charge
κ^{-1}	Debye length
$T = 298$ K	temperature
k_B	Boltzmann's constant
N_A	Avogadro's number
ξ_{reg} =1 or 0 (on/off)	charge regulation
n_p	protonated residues
pK_a =see Table II	acid dissociation constant
$\xi_{surf} = 1$ or 0 (on/off)	G-C potential
$\Phi_0 = \frac{2k_BT}{q} \sinh^{-1}$ $* \sqrt{\rho(8k_BTc_0\varepsilon_0\varepsilon_r)}$	potential at the surface
$\rho = -0.053$ C/m^2	surface charge density
d_i	distance to the surface
$k_h = 0.76\ k_BT$	spring constant
R_i	bond length
$R_e = 4.9$ Å	equilibrium bond length
$n_b = n - 1$	number of bonds
$\varepsilon_{Zn} = 4.57\ k_BT$	strength of SR
n_H	number of HIS
$d_{Zn-H} = 2.4$ Å	bound Zn(II)-HIS distance

Table II: Stoichiometric (pK_a^*) and intrinsic (pK_a) acid dissociation constants of residues at 0 mM, 80 mM and 150 mM 1:1 salt

Residue id		1	2	3	4	5	6	7	8	9	10	11	12
Residue	NTR[a]	ASP	SER	**HIS**	ALA	LYS	ARG	**HIS**	**HIS**	GLY	TYR	LYS	ARG
pKa	7.5	4.0	-	6.3	-	10.4	12.0	6.3	6.3	-	9.6	10.4	12.0
pKa^*(0 mM)	7.3	1.7	-	**5.2**	-	10.0	12.5	**4.0**	**4.5**	-	8.1	10.3	12.8
pKa^*(80 mM)	7.6	3.2	-	**6.0**	-	10.2	12.2	**5.4**	**5.7**	-	8.9	10.4	12.3
pKa^*(150 mM)	7.7	3.4	-	**6.1**	-	10.2	12.1	**5.6**	**5.8**	-	9.1	10.4	12.2

[a] NTR and CTR are abbreviations for N and C terminals, respectively.

Residue id	13	14	15	16	17	18	19	20	21	22	23	24	
Residue	LYS	PHE	**HIS**	GLU	LYS	**HIS**	**HIS**	SER	**HIS**	ARG	GLY	TYR	CTR[a]
pKa	10.4	-	6.3	4.4	10.4	6.3	6.3	-	6.3	12.0	-	9.6	2.6
pKa^*((0 mM)	9.9	-	**5.1**	1.3	11.0	**4.5**	**5.0**	-	**5.0**	13.0	-	9.5	1.0
pKa^*((80 mM)	10.0	-	**6.0**	3.2	10.7	**5.7**	**5.9**	-	**5.8**	12.3	-	9.7	2.2
pKa^*(150 mM)	10.1	-	**6.2**	3.4	10.7	**5.8**	**5.9**	-	**5.9**	12.3	-	9.8	2.3

Table III: Concentrations (mM) of explicit divalent and implicit monovalent ions and corresponding Debye lengths, $1/\kappa$

	Na^+	Cl^-	Ca^{2+}	Zn^{2+}	κ^{-1} (Å)
(a)	80	80	0	0	10.8
(b)	61.55	73.85	6.15	0	11.7
(c)	61.55	74.35	6.15	0.25	11.7

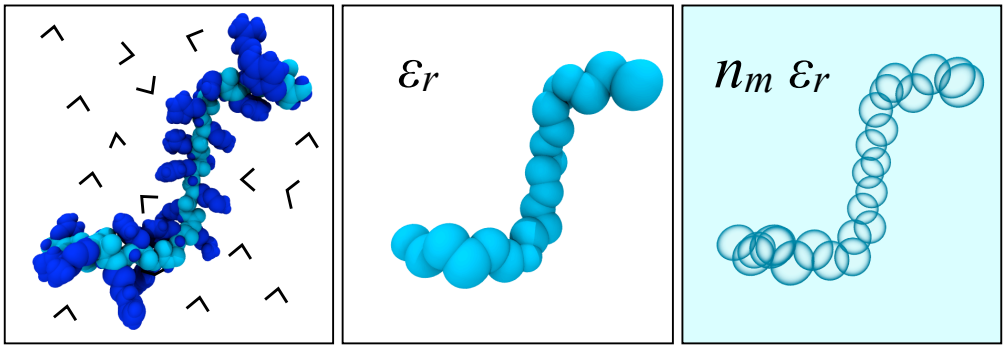

Figure 1: Models in decreasing order of detail, left to right: Atomistic (MD), soft sphere amino acid bead model (MC), and hard sphere amino acid model (DFT).

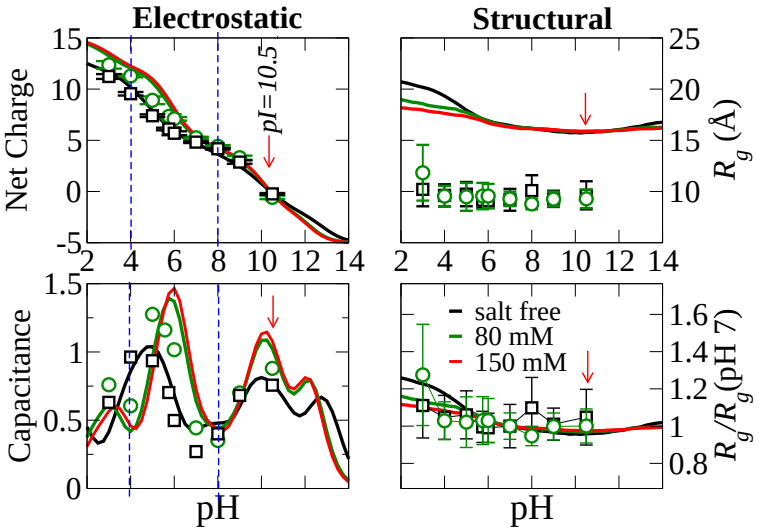

Figure 2: Electrostatic and structural properties of His5 as a function of pH and 1:1 salt concentration calculated using MC (lines) and MD (symbols) simulations. The interval fenced by the dashed lines shows saliva conditions.

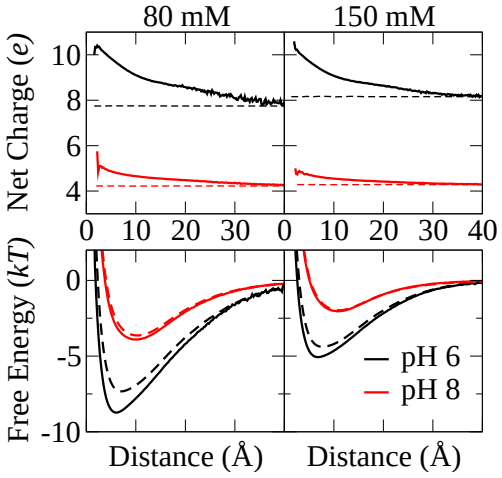

Figure 3: Net charge and interaction free energy of His5 as a function of distance from a surface with a charge density $\rho = -300$ Å$^2/e$ with (solid lines) and without (dashed lines) charge regulation at pH 6 and pH 8 where the capacitance is maximized and minimized, respectively.

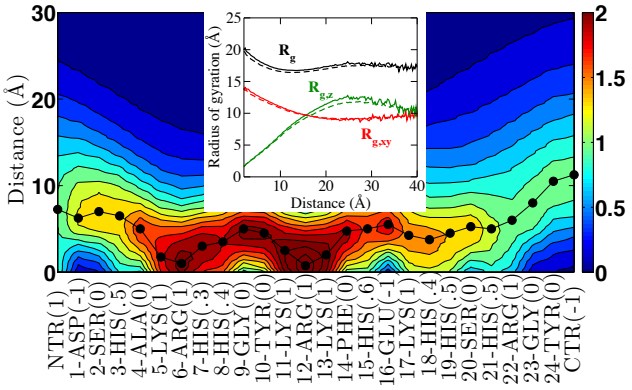

Figure 4: Residual concentration profile in mM as a function of the distance from the surface at pH 6 and 80 mM 1:1 salt. *Inset*: Radius of gyration and its components with (solid) and without (dashed) charge regulation. Circles indicate the most probable location of each residue relative to the surface and average bulk charges are shown in parentheses.

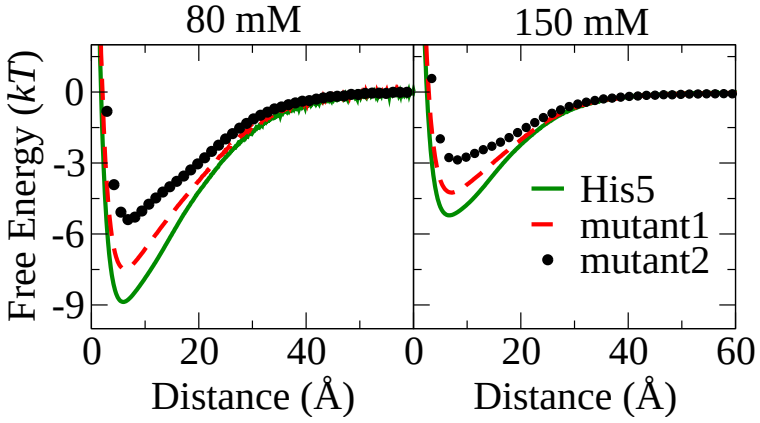

Figure 5: Interaction free energy of His5 (solid lines), mutant1 (dashed lines, 12-ARG is replaced by a negative TYR) and mutant2 (circles, primary ARG-LYS patch is mutated to a neutral GLY) at pH 6 and 80 mM 1:1 salt solution.

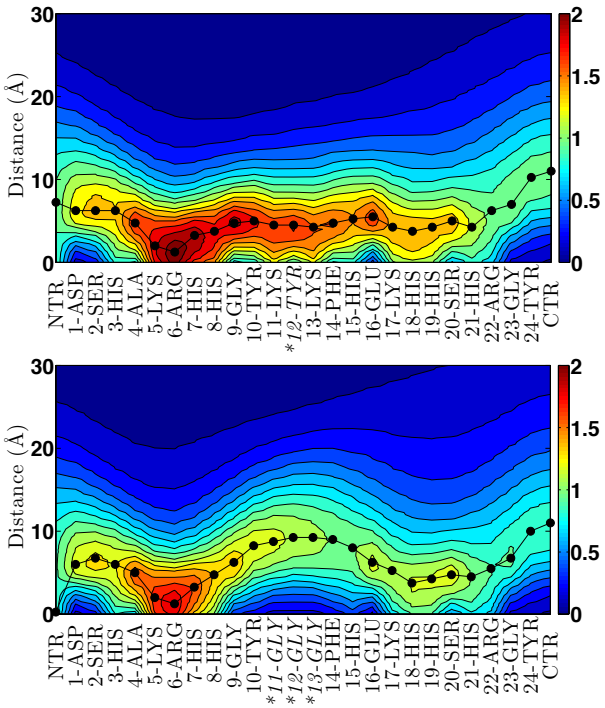

Figure 6: Concentration profiles of mutant1 (*top*) and mutant2 (*bottom*) at pH 6 and 80 mM 1:1 salt solution as a function of the distance from the surface. Mutated amino acids are indicated by *. Circles show the most probable positions of residues relative to the surface.

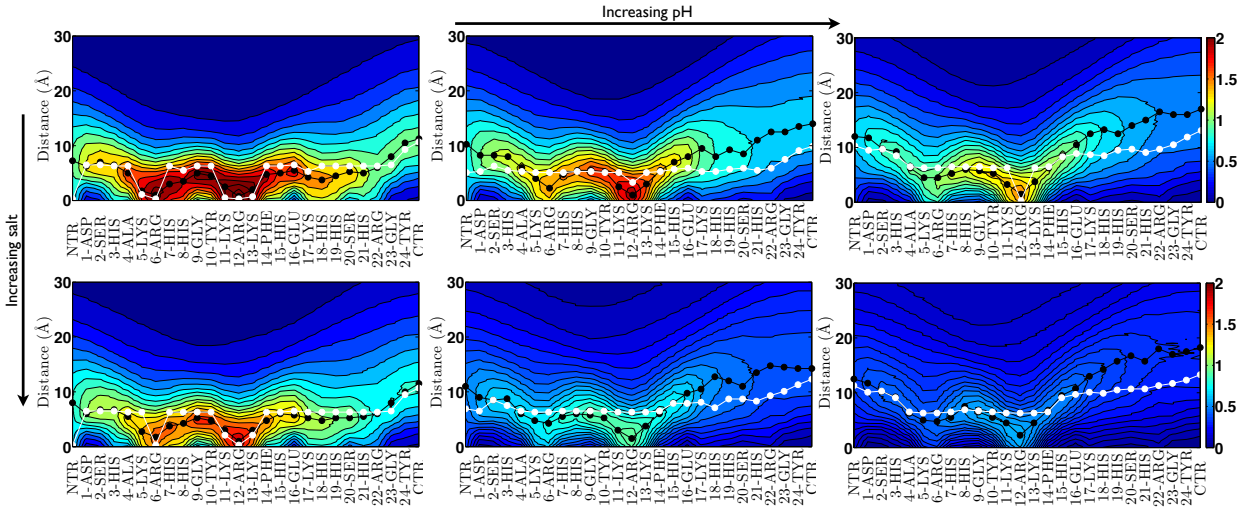

Figure 7: Residual concentration profile in mM as a function of distance from the surface at pH 6, 7, and 8; in 80 mM and 150 mM 1:1 salt. White and black circles show the most probable positions of residues relative to the surface predicted by MC and DFT, respectively.

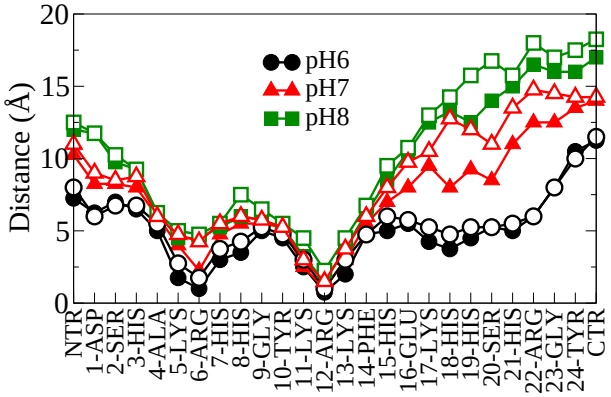

Figure 8: Most probable positions of residues relative to the surface at 80 mM (full symbols) and 150 mM (open symbols)

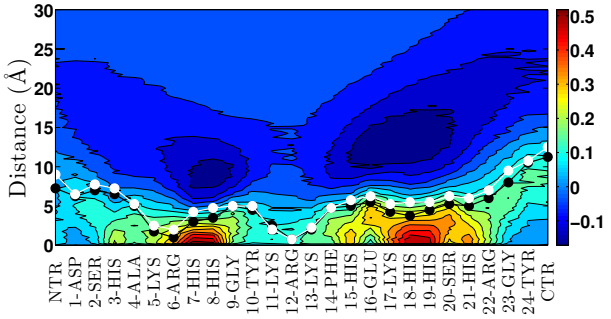

Figure 9: Difference between the residual concentration profiles with and without charge regulation at pH 6 and 80 mM 1:1 salt solution. The most probable positions of residues with and without charge regulation are shown by black and white circles, respectively.

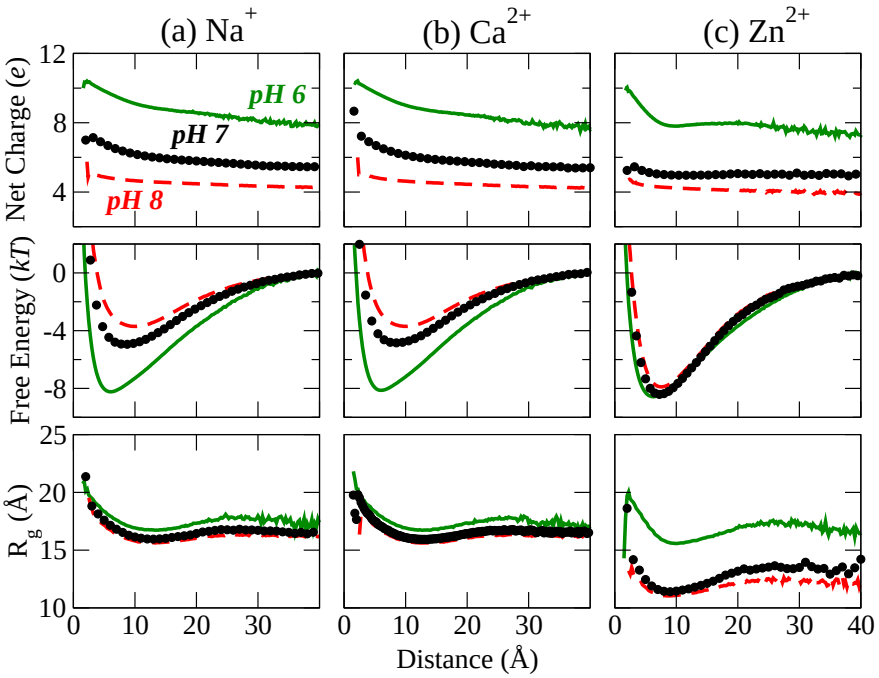

Figure 10: Properties of His5 as a function of the surface distance at 80 mM total ionic strength with and without divalent ions. See Table III for the concentration of divalent ions.

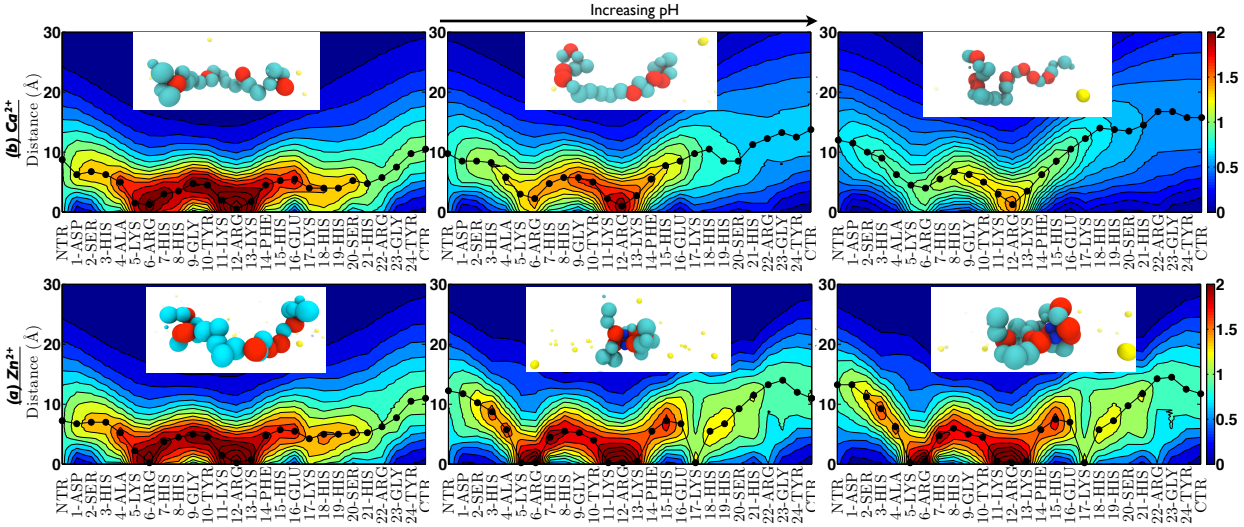

Figure 11: Concentration profiles of residues with explicit divalent ions at pH 6, 7 and 8 and 80 mM total ionic strength. Deprotonated HIS (red), calcium (yellow) and zinc (blue) ions are shown in the snapshots of His5 conformation on the surface